Hindawi
Advances in Materials Science and Engineering
Volume 2022, Article ID 8446392, 16 pages
https://doi.org/10.1155/2022/8446392

Research Article

Study of Problems Related to Laying Ballastless Track in the Turnout of Ballasted Track at High-Speed Railway Stations

Ma Xue-Ning, Hao Zi-Xiang, Liu Chang, Wang Xu, and Wang Bo-Lin

College of Civil Engineering, Lanzhou Jiaotong University, Lanzhou, Gansu 730070, China

Correspondence should be addressed to Ma Xue-Ning; 65809626@qq.com

Received 16 February 2022; Revised 11 May 2022; Accepted 12 May 2022; Published 28 May 2022

Academic Editor: Jinyang Xu

Due to the complex dynamic interactions of the vehicle-track system in the turnout of high-speed railway stations on a ballasted track, the geometric position of the line changes rapidly. In order to improve the stability of the line, the ballasted track in the turnout area of the stations can be replaced by a ballastless track. Based on the engineering background of laying ballastless track in the turnout area of Zhonglan's high-speed railway station, this paper studies the subgrade reinforcement scheme, subgrade settlement prediction, and ballasted-ballastless track transition section setting. The result shows that, in order to meet the requirements of laying ballastless track in the turnout area, a reinforcement scheme of subgrade impact rolling, surcharge preloading, and closed water isolation on the subgrade surface is proposed. Based on the commonness and individuality of the grey Verhulst, hyperbola, and Deng Yinger prediction model, this paper optimizes the combination of the three models. The sum of squares of the minimum errors of the combined model is used as the objective function to solve the optimal weighting coefficient, and in this way the combined prediction model is constructed. Through the prediction comparison, we found that the accuracy of the three-model combination prediction model is better than any single- or two-model combination, and its adaptability and reliability are stronger and more reliable. This dynamic analysis model of vehicle tracks was established to carry out the dynamic response analysis under the conditions of fastener stiffness grading transition and ballast glue grading curing ballast bed transition. The results show that the dynamic response indexes under the two transition modes meet the requirements for the smooth running of trains. Due to the convenience of fastener stiffness transition construction and easier replacement, this measure is recommended.

1. Introduction

In recent years, due to the dynamic interactions of vehicle-rail systems and the complexity of drainage system [1, 2], and the influence of the special engineering properties of loess, the geometric position of the turnout area of some newly built high-speed railway stations with a ballast track in northwest China has changed rapidly after the operation of the line, and the maintenance is difficult and the work efficiency is low [3]. In order to improve the stability of the line and reduce the difficulty and frequency of maintenance operations, on the basis of not changing the overall design scheme of the whole track bed and not increasing investment by a lot, it is very important to study the laying of ballastless track in the turnout area of the station by drawing on lessons from the uneven settlement of the turnout area of the pre-opened line station.

The two key technical problems of ballastless track laying in turnout area of high-speed railways with ballast tracks are to reinforce the subgrade to strictly control its post-construction settlement in the turnout area to meet the requirements of laying ballastless track and to solve the problem of setting the transition section of ballasted-ballastless track to ensure the safe and smooth passage of vehicles.

According to the "high-speed railway design specifications" [4], the design standard for the post-construction settlement of a ballasted track with a high-speed railway subgrade for a speed of 250 km/h is less than 100 mm, and the post-construction settlement design standard for the ballastless track subgrade is less than 15 mm. Therefore, it is necessary to take effective measures to reinforce the subgrade in the turnout area of ballasted track, and to predict

the subgrade settlement to verify whether the post-construction settlement meets the requirements of laying a ballastless track.

At present, the prediction methods for the settlement of a high-filled subgrade mainly include the empirical formula derivation method, numerical simulation method, and curve fitting method [5–13]. The commonly used curve fitting methods include the hyperbolic method, grey prediction method, grey theory-Markov method, power function method, exponential equation method, and Asaoka method. The settlement of a high-filled subgrade is a complex process related to the environmental conditions of the foundation, the stress history of the foundation soil, the engineering properties of the embankment filling, the height of the embankment filling, and the construction technology [14]. The focus of each model mentioned above is different, so it is difficult to use a single prediction model to make an accurate prediction of settlement, resulting in low confidence in the prediction's accuracy. In order to comprehensively utilize the effective information contained in each model and improve the prediction's accuracy, some scholars have put forward a combined prediction method, and therefore two-model combined model is more commonly used [15–20].

The purpose of setting the transition section of the ballasted-ballastless track is to alleviate the problems of excessive stiffness differences under the track and the dynamic irregularity of the line. Experts and scholars have put forward many treatment measures for the transition section [21], such as setting an auxiliary track, widening the sleeper width, increasing the sleeper length, increasing the track bed thickness, changing the fastener stiffness, and curing the track bed with ballast glue. In this specific application, it is found that setting the auxiliary rail will have a certain transition effect only after the large settlement of the line. Changing the sleeper size will affect the operation of large machines, which are rarely used. Increasing the thickness of track bed will affect the stability of the line and such an increase is difficult to implement. The method of changing the fastener stiffness by stages in the transition section can significantly reduce the vibration caused by train operations. Adopting the method of a graded curing track bed will improve the overall performance and vertical stiffness of track bed and the transverse and longitudinal resistance of the track. Both of these two methods have the same characteristics of simple operation, high efficiency, and convenient maintenance and replacement, and they have been widely used in practical engineering.

Based on this background, combined with the laying of ballastless track in the turnout area of a ballasted track high-speed railway station under construction, and based on the design standard of a ballasted track subgrade and the current embankment construction progress (filled to the bottom layer of the subgrade bed), this paper puts forward the plan for a subgrade reinforcement in order to reduce the post-construction settlement of the subgrade in the turnout area of the station.

Then, this paper proposes a method for constructing the combined prediction model. Combined with the field monitoring settlement data, the single model and the combined model are used to predict the subgrade's settlement, and the prediction accuracy of each model is evaluated.

Finally, through dynamic analysis of the vehicle track, the dynamic response indexes of the fastener stiffness graded transition and the ballast glue graded curing track bed transition in the transition section are evaluated. These research results can provide technical support for the engineering application of laying a ballastless track in the turnout area.

2. Project Overview and Subgrade Reinforcement Scheme

The Zhongwei-Lanzhou passenger dedicated line is a high-speed railway connecting Zhongwei City in the Ningxia Hui Autonomous Region and Lanzhou City of Gansu Province. It is an important part of China's "eight vertical and eight horizontal" railway network. It is a ballasted track railway supporting a speed of 250 kilometers per hour, and the opening date is at the end of 2022. The current plan is to lay ballastless tracks in the turnout areas of Beitan and Pingchuan stations, both of which are located in Baiyin City, Gansu Province.

2.1. Overview of Beitan Station. The starting and ending mileages of the Beitan station are Dk84 + 750 ~ Dk86 + 650. The maximum filling height of the line is about 13.2 m. The station is located in the Piedmont and intermountain alluvial proluvial inclined plain, with a local aeolian landform that is flat and open terrain. According to the geological survey and exploration, the formation lithology is mainly sandy loess and fine sand of Quaternary Holocene Aeolian diluvium and sandy loess and fine sand and coarse sands of upper alluvial diluvium. The physical and mechanical indexes of each stratum are shown in Table 1. According to the different thicknesses of collapsible loess at the embankment base, the foundation treatment scheme is reinforced by measures such as impact rolling, dynamic compaction, and a cement soil compaction pile. The cement soil compaction pile, with a diameter of 0.4 m and a spacing of 1.0 m, is arranged in an equilateral triangle with a pile length of 6~8 m.

2.2. Overview of Pingchuan Station. The starting and ending mileages of the Pingchuan station are Dk122 + 994.15 ~ Dk125 + 053.58, and the maximum filling height of the subgrade is 16.33 m. The construction site is located in the piedmont alluvial proluvial plain area in a flat and open terrain. The formation lithology is mainly sandy loess, silt, gravel sand, and fine breccia soil of Quaternary Holocene alluvial diluvium. The physical and mechanical indexes of each stratum are shown in Table 2. Sandy loess is collapsible and belongs to grade I slight non-self-weight collapsibility. The thickness of collapsible soil layer is about 1~2.4 m. The design scheme of the foundation treatment is surface cleaning and impact rolling.

Table 1: Soil parameter of the Beitan station.

Material	Thickness(m)	γ(kN m)$^{-3}$	c(kPa)	$(\varphi)^{\circ}$	Es(MPa)	σ_0(kPa)
Fine sand ($Q_4^{eol+pl4}$)	0.5–3.2	16.8	4.5	26.3	5.3	100
Sand loess ($Q_4^{eol+pl3}$)	1.0–12.7	17.2	13.8	22.6	9.34	150
Sand loess (Q_4^{al+pl3})	0.8–21.0	17.4	16.2	23.2	8.10	150
Fine sand (Q_4^{al+pl4})	1.1–8.0	17.8	6.5	32.6	11.3	230
Coarse sands (Q_4^{al+pl5})	2.5–11.4	18.7	5.7	34.2	18.1	370

Table 2: Soil parameter of Pingchuan station.

Material	Thickness(m)	γ(kN m)$^{-3}$	c(kPa)	$(\varphi)^{\circ}$	Es(MPa)	σ_0(kPa)
Sand loess (Q_4^{al+pl3})	1–2.4	17.5	11.5	20.4	4.6	150
Silty sand (Q_4^{al+pl4})	2.0–7.0	17.2	5.3	27.2	7.4	210
Gravelly sand (Q_4^{al+pl5})	1.8–3.5	18.8	6.5	33.5	12.8	270
Fine breccia soil (Q_4^{al+pl6})	1.0–7.3	19.2	8.5	35.7	22.4	300

2.3. Subgrade Reinforcement Scheme. In order to improve the line stability in the turnout area of the station and reduce the difficulty and frequency of maintenance, the construction party is putting forward the scheme of laying a ballastless track in the turnout area. When this changes, the foundation treatment of the two stations has been completed, and the embankment is filling the bottom layer of the subgrade bed. In order to reduce the post-construction settlement of subgrade in turnout area and meet the requirements of laying ballastless track, the following reinforcement scheme is proposed.

(1) After the completion of filling the bottom layer of the subgrade bed in the turnout area and transition section, the top surface of the bottom layer of the subgrade bed will be compacted by impact compaction for no less than 40 times.

(2) After the impact rolling is completed, surcharged preloading will be carried out. The height of the preloaded soil is 3 m, and the preloading time is generally not less than six months.

(3) Before filling the surface layer of the subgrade bed, a 0.20 m-thick composite geomembrane with medium coarse sand is put on the top surface of the bottom layer of the subgrade bed.

(4) The upper 0.2 m of the surface layer of the subgrade bed is filled with graded crushed stone mixed with 5% cement, and the lower 0.5 m is filled with just graded crushed stone.

(5) C25 concrete is used for cast-in-situ sealing between the embankment slope's toe and drainage ditch, with a thickness of 0.12 m.

3. Settlement Deformation Observation

In order to accurately obtain the settlement level of the subgrade in the turnout area, the design side makes the settlement monitoring section with a spacing of 25 m. Three settlement observation piles are set for the monitoring sections that are arranged at the center of the subgrade and the shoulders on both sides. One settlement plate is set at the base of the center of subgrade. The settlement observation of the Beitan Station began on October 24, 2019, and preloading began on June 16, 2020. By September 20, 2020, due to track laying and other reasons, the preloading filling was removed, and the settlement data of 20 sections were obtained. The settlement observation at the Pingchuan Station began on April 26, 2020, and ended on October 23, 2020. The settlement data of 22 sections were obtained without preloading due to girder erection and track laying. Due to space limitations, the settlement plate data of the three sections at the two stations were selected for analysis: DK84 + 771, DK84 + 821, and DK123 + 690, respectively. The embankment filling heights are 13.23 m, 11.91 m, and 6.0 m, respectively. Figure 1 is the measured fill height-time-settlement curve.

As can be seen from Figure 1, the settlement of the DK84 + 771 and DK84 + 821 sections increases with the increase of time and filling height, showing a good curve shape. Also, the settlement has converged. The measured maximum settlement of the two sections was 6.1 mm and 13.48 mm, respectively. The maximum settlement before preloading was 5.4 mm and 10.52 mm, respectively. At the end of preloading, the settlement of the two sections was 6.07 mm and 13.45 mm, respectively. The settlement of the two-section subgrade after preloading was 99.5% and 99.8% of the current total settlement, respectively, indicating that the settlement of the subgrade after preloading is stable. The settlement curve of the DK123 + 690 section is gentle in the filling stage. In the later stage, the settlement has stabilized and converged under the repeated rolling of the beam carrier with a large quality. The measured maximum settlement is 3.9 mm, and the settlement is 3.5 mm when the filling is completed, accounting for about 89.7% of the total settlement. As can be seen from the measured settlement of the three sections, most of the subgrade settlement occurs in the filling stage.

4. Settlement Prediction and Accuracy Evaluation

This paper introduces the basic principles of three single settlement prediction models: grey Verhulst model (V

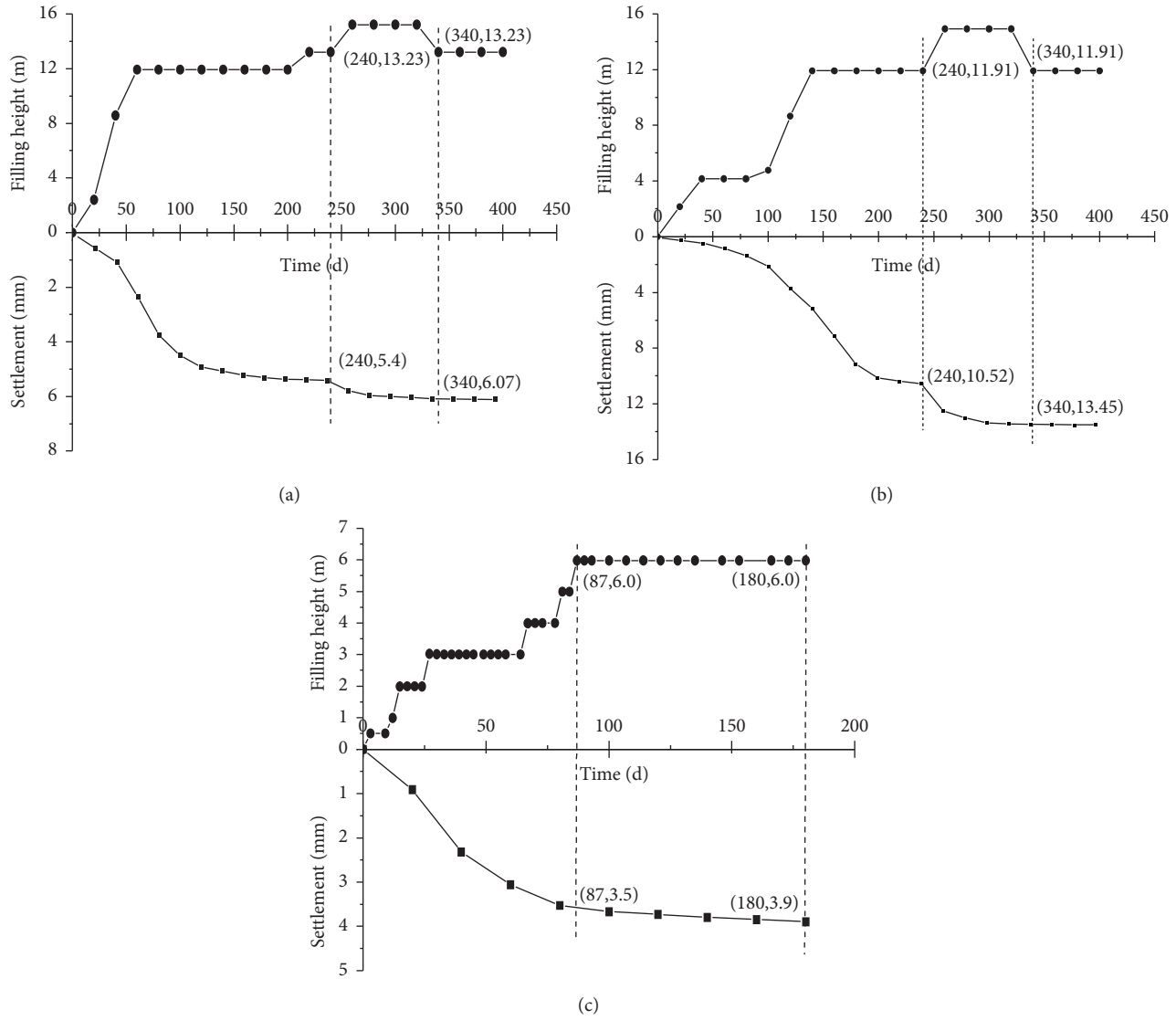

Figure 1: Subgrade filling height-settlement-time curve. (a) DK84 + 771. (b) DK84 + 821. (c) DK123 + 960.

model), hyperbolic model (H model), and Deng Yinger model (D model). Then, considering the advantages and specific limitations of the three single settlement prediction models, a new combination model is established by optimizing the combinations of the D-H model, D-V model, H-V model, and D-H-V model. Based on the measured settlement data of the three sections, the prediction results of different models are compared, and the optimal model for the prediction of subgrade settlement is obtained.

4.1. Introduction of Three Settlement Prediction Models

4.1.1. Grey Verhulst Model (V Model). The basic idea of the V model is that the number of biological individuals increases exponentially. Limited by the surrounding environment, their growth rate gradually slows down and finally stabilizes at a fixed value. The V model has a good performance and provides an effective and feasible method for the prediction and control of subgrade settlement.

Assuming that there is a known measured sequence $x^0_{(i)}$, $i = 1, 2, \ldots n$, the measured sequence $x^0_{(i)}$ is accumulated to obtain the sequence $x^1_{(i)}$:

$$x^{(1)}_{(i)} = \sum_{k=1}^{i} x^{(0)}_{(k)}. \tag{1}$$

The differential equation is established based on $x^1_{(i)}$ and the V model is obtained:

$$\frac{dx^{(1)}}{dt} = ax^{(1)} - b\left(x^{(1)}\right)^2. \tag{2}$$

In the formula, a is the development coefficient and b is the grey action, which can be solved by the least square method and the extreme value principle. The specific solution process can be found in the literature [7].

The solution of differential (2) is

$$x_{(1)}^{(t)} = \frac{a/b}{1 + \left(a/bx_{(0)}^{(1)} + 1\right)e^{-at}}. \quad (3)$$

In the formula, $x_{(0)}^{1}$ is the first digit of the observation sequence, $x_{(1)}^{t}$ is the cumulative settlement value at the corresponding t time.

4.1.2. Hyperbolic Model (H Model). The H model considers that the curve of subgrade settlement variation with time is similar to the hyperbolic curve, which can be used to fit the curve of settlement variation with time, and the empirical formula of settlement variation with time is obtained. The basic equation is:

$$S_t = S_0 + \frac{t - t_0}{\alpha + \beta(t - t_0)}. \quad (4)$$

In the formula, S_0 is the settlement at time t_0. S_t is the settlement at time t. And α and β are undetermined parameters.

4.1.3. D Model. The D model is a new model proposed by Deng Yinger. It summarizes the Poisson curve model and Verhulst model, which can accurately predict the variation of the whole process settlement [22]. Its basic equation is:

$$S = \frac{b_1}{1 + b_2 \exp\left(-b_3 t^{b_4}\right)}. \quad (5)$$

In the formula, b_1, b_2, b_3, and b_4 are all parameters to be determined, and when $b_4 = 1$, it is a Poisson curve model.

4.2. Establishment of Combination Forecasting Model. Different prediction methods can be used to predict the settlement of high-fill subgrade. Because of the different applicable conditions of each method, the prediction results and accuracy are also different. However, each single model has its own unique features with different emphases, and its prediction results have certain value. If some prediction methods with large errors are abandoned, some important information will be lost. In order to comprehensively use the effective information contained in each single model, some scholars have proposed a combination forecasting method. This method combines two or more different single models by some combination principle to form a new model.

In practical engineering, when the measured settlement curve is smooth and regular, the single model can better predict the settlement, and the prediction accuracy is high. However, when the settlement curve is complex (such as curve turning, steep drop, or S type) or the regularity is poor, the prediction error of the single model is larger, but the combination model has a better prediction effect. This is because it is difficult to use one or two simple functions to express complex curves. Only by combining different simple functions, the line shape of complex curves can be better expressed.

The key of the combined model is to determine the weight of each single model that constitutes the combined model. At present, the methods for determining the weight are mainly divided into the fixed weight determination method and the variable weight determination method. Since the variable weight determination method is relatively complex and has a large number of calculations, the weight of the combined model is mainly determined by the fixed weight determination method [20, 21]. In this paper, the fixed weight determination method is used to optimize the combination of the above three individual models, and the minimum sum of squares of error of the combined model is used as the objective function to determine the weight of each combined model. The modeling process is as follows.

Denote Y_t $(t = 1, 2, \ldots, n)$ as the measured value of the settlement of a high-filled subgrade, assuming that there are m kinds of prediction models, which are $\widehat{Y}_1$, $\widehat{Y}_2$,..., $\widehat{Y}_m$, where the predicted value of $\widehat{Y}_i$ is $\widehat{Y}_{i1}$, $\widehat{Y}_{i2}$,..., $\widehat{Y}_{in}$ $(i = 1, 2, \ldots, m)$. Then, the error of the i prediction method in the t data is $e_{it} = Y_t - \widehat{Y}_{it}$ $(i = 1, 2, \ldots, m; t = 1, 2, \ldots, n)$. If k_i is used to represent the weight of the method i in the combination model, then the combination model Y is

$$Y = \sum_{i=1}^{m} k_i \widehat{Y}_{it}, \quad t = 1, 2, \ldots, n. \quad (6)$$

The weight of the combined model satisfies $\sum_{i=1}^{m} K_i = 1$, and the errors of combined model is

$$e_t = Y_t - \widehat{Y}_t = \sum_{i=1}^{m} k_i Y_t - \sum_{i=1}^{m} k_i \widehat{Y}_{it} = \sum_{i=1}^{m} k_i e_{it}, \quad t = 1, 2, \ldots, n. \quad (7)$$

The weighted vector of the combination model is denoted as $K = (k_1, k_2, \ldots k_m)^T$, and prediction error vector of the i prediction method is $E_i = (e_{i1}, e_{i2}, \ldots, e_{in})^T$, then the error matrix of m prediction methods is $e = (E_1, E_2, \ldots, E_m)^T$. When the sum of squares of prediction errors of the combined prediction method is A, there are

$$\begin{aligned} J &= \sum_{t=1}^{n} e_t^2 = \sum_{t=1}^{n} \left(\sum_{i=1}^{m} w_i e_{it} \right)^2 \\ &= \sum_{t=1}^{n} \left(\sum_{i=1}^{m} \sum_{j=1}^{m} w_i w_j e_{it} e_{jt} \right) = \sum_{i=1}^{m} \sum_{j=1}^{m} w_i w_j \left(\sum_{t=1}^{n} e_{it} e_{jt} \right). \end{aligned} \quad (8)$$

The error information matrix of the combined model is

$$E = e^T e = \begin{pmatrix} \sum_{t=1}^{n} e_{1t}^2 & \sum_{t=1}^{n} e_{1t} e_{2t} & \cdots & \sum_{t=1}^{n} e_{1t} e_{mt} \\ \sum_{t=1}^{n} e_{2t} e_{1t} & \sum_{t=1}^{n} e_{2t}^2 & \cdots & \sum_{t=1}^{n} e_{2t} e_{mt} \\ \vdots & \vdots & \cdots & \vdots \\ \sum_{t=1}^{n} e_{mt} e_{1t} & \sum_{t=1}^{n} e_{mt} e_{2t} & \cdots & \sum_{t=1}^{n} e_{mt}^2 \end{pmatrix} = E_{ij}. \quad \text{Let}$$

$\sum_{t=1}^{n} e_{it} e_{jt} = E_{ij}$ denotes the product of the prediction error of the i th prediction method and the j th prediction method on the n th data, then the sum of error squares of the combined prediction model can be represented by this matrix:

$$J = K^T E K. \quad (9)$$

If each prediction method is independent of the others, then the prediction error vector $E_i = (e_{i1}, e_{i2}, \ldots, e_{in})^T$ of

each prediction method is linearly independent, and E is a positive definite matrix, and then the matrix is invertible. Note $R = (1, 1, \ldots, 1)^T$, then the weight normalization condition $\sum_i^m k_i = 1$ can be expressed as $R^T K = 1$ by the matrix. So, the combined forecasting problem can be expressed as a nonlinear programming model.

$$\begin{aligned} &\min J = K^T E K, \\ &R^T K = 1. \end{aligned} \tag{10}$$

To solve the above minimum problem, the Lagrange multiplier λ can be introduced to construct the following equation:

$$J = K^T E K + \lambda\left(R^T K - 1\right). \tag{11}$$

The condition for the existence of extreme value is that the first derivative of J to K is zero, namely,

$$\frac{\partial J}{\partial K} = 0 = 2EK + \lambda R. \tag{12}$$

With E^{-1} left multiplication $\partial J/\partial K = 0 = 2EK + \lambda R$ two ends to get $2K + \lambda E^{-1} R = 0$. Then, with R^T left multiplication both ends of this formula to get $2R^T K + \lambda R^T E^{-1} R = 0$, which can be:

$$\lambda = \frac{2}{R^T E^{-1} R}. \tag{13}$$

Substituting (13) into (12), the expression of weight vector is

$$K = \frac{E^{-1} R}{R^T E^{-1} R}. \tag{14}$$

4.3. Accuracy Evaluation of Prediction Model. In order to further explore the accuracy, applicability, and reliability of each prediction model, the absolute error sum of squares (SSE), standard error (SE), relative error sum of squares (SSPE), relative standard error (SPE), and average absolute percentage error (MAPE) are used to evaluate the accuracy of each prediction model to explore the advantages and disadvantages of each prediction model. The calculation formulas of each parameter are as follows:

$$\begin{aligned} \mathrm{SSE} &= \sum_{t=1}^{N} \left(\widehat{y}_t - y_t\right)^2, \\ \mathrm{SE} &= \left(\frac{\mathrm{SSE}}{N}\right)^{0.5}, \\ \mathrm{SSPE} &= \sum_{t=1}^{N} \left(\frac{\widehat{y}_t - y_t}{y_t}\right)^2, \\ \mathrm{SPE} &= \left(\frac{\mathrm{SSPE}}{N}\right)^{0.5}, \\ \mathrm{MAPE} &= \frac{1}{n} \sum_{t=1}^{N} \left(\frac{\left|\widehat{y}_t - y_t\right|}{y_t}\right) \times 100\%. \end{aligned} \tag{15}$$

According to the MAPE value, the prediction accuracy can be divided as shown in Table 3.

4.4. Optimal Prediction Model. According to the basic principle of establishing a combination model, four combination models are obtained based on three single models, namely, D-H model, D-V model, H-V model, and D-H-V model. The optimal weight coefficients of each combination model of three sections are calculated by formula (14), as shown in Table 4. It can be seen that the larger the weight coefficient is, the larger the proportion of the model in the combined model is. Three single models and four combined models are used to predict the measured settlement of three sections, and the predicted curves are shown in Figure 2. The evaluating indexes of each prediction model can be calculated from formula (15), as shown in Table 5. The relationship curve between observation time and relative error of each section and the scatter plot of observation time and residual error are shown in Figures 3 and 4, respectively.

From Figure 2, it can be seen that the deviation between the predicted settlement and the measured settlement is large in the early stage of loading, but with the extension of monitoring time, the predicted value and the measured value are closer and closer. Overall, due to the different applicability of each model, the prediction accuracy is also different, but the error of final settlement predicted by combined model is smaller than that of single model.

It can be seen from Figure 3 that whether it is a single model or a combined model proposed in this paper, the relative error between the actual settlement value of early monitoring and the predicted value of each prediction model is large. For example, in the DK84 + 711 section, when the monitoring time is 40 d, the relative errors of D model, H model, and the combined prediction D-H-V model are 176.42%, 109.70%, and 51.98%, respectively. But in practical engineering, scholars generally pay more attention to the final settlement without considering the early error. As long as the observation data points exceed the inflection point of the curve, the prediction results have considerable accuracy. For example, when the monitoring time exceeds 200 days, the relative error is within 6.5%, so the settlement of high fill can be estimated by the prediction model. It can be seen from Figure 4 that the variation law of residual plot conforms to the characteristics of randomness and unpredictability, and the residual values are randomly distributed up and down the line with zero residual. In comparison, the combined model proposed in this paper has better prediction effect. As can be seen from Table 3, in DK84 + 771 section, the MAPE values of three single prediction models are 26.35%, 17.30%, and 8.58%, respectively. According to the precision classification standard, the D model belongs to a feasible prediction, the H model belongs to a good prediction, and the V model belongs to a high-precision prediction. In the DK84 + 821 section, the MAPE values of the D model and the V model are 7.34% and 9.73%, and belong to the high-precision prediction, while the MAPE value of the H model is 45.99%, which belongs to the feasible prediction. According to the SSE and SE values of

Table 3: Classification of MAPE prediction grades [17].

MAPE (%)	Prediction grade	MAPE (%)	Prediction grade
<10	High precision	20~50	Feasible
10~20	Good precision	>50	Infeasible

Table 4: Optimal weight coefficient of combined prediction model.

Combination model	Beitan station						Pingchuan station		
	DK84 + 771 section			DK84 + 821 section			DK123 + 960 section		
	k_1	k_2	k_3	k_1	k_2	k_3	k_1	k_2	k_3
D-H	0.0773	0.9227	—	0.9993	0.0007	—	0.9972	0.0027	—
D-V	0.1492	—	0.8508	0.9974	—	0.0026	0.9943	—	0.0057
H-V	—	0.2899	0.7101	—	0.2482	0.7518	—	0.2585	0.7415
D-H-V	0.0334	0.2557	0.7109	0.9965	0.0008	0.0027	0.1202	0.0028	0.8769

the three single models, the prediction effect of the DK84 + 771 section is in the order of V model > H model > D model, and the prediction effect of the DK84 + 821 section is in the order of D model > V model > H model. The same can be obtained in the DK123 + 960 section and the three single model prediction effect is: V model > D model > H model. It can be seen from the optimal weight coefficients of each combination model in Table 4 that the smaller the error of the single model is, the larger the weight of the single model in the combination model is, and the larger the error of the single model is, and the corresponding error of the combination model composed of it is also larger.

It can be seen from Figures 3 and 4, and Table 5 that the residuals of each combination model are small, especially in the later period when the residual is basically zero, which is very conducive to the prediction of subgrade settlement. For the DK84 + 771 section, the MAPE values of the H-V and D-H-V models are less than 10%, which belongs to high-precision prediction. The D-V and D-H-V models in the DK84 + 821 section belong to high-precision prediction. In DK123 + 960 section, the four combination models belong to high-precision prediction. It can also be seen that if the MAPE value in the combined model is small, its SSE and SE are always smaller than those of any single model that constitutes the combined model. The error evaluation index of the three-model combination model is less than that of the two-model combination model and single model. According to the SSPE value and SPE value of the indexes evaluating the stability and reliability of the model, the SSPE value and SPE value of the combined prediction model belonging to the high-precision prediction are lower than those of each single model, indicating that the combined prediction model is more reliable and adaptable. According to the prediction results of the above three sections, the three-model combination model is the optimal settlement prediction model.

4.5. Calculation of Post-Construction Settlement. The post-construction settlement of ballastless track subgrade should meet the requirements of line smoothness, structural stability, and fastener adjustment ability, and the post-construction settlement should not exceed 15 mm. Using the above optimal settlement prediction model (three-model combination model), the post-construction settlement of the three sections is predicted. The prediction results are shown in Table 6. It can be seen that the post-construction settlement of the three sections is less than 15 mm, which meets the requirements of laying ballastless track.

5. Dynamic Response of Ballasted-Ballastless Track Transition Section

The structural stiffnesses of ballastless track and ballasted track are quite different, and so it is necessary to set the transition section of ballasted-ballastless track to ensure the uniform transition of under-rail stiffness. In this paper, the fastener stiffness transition and ballast glue curing ballast bed transition are selected, and the two methods are arranged in a three-stage transition form. The vehicle-track vertical dynamic analysis model is established to analyze the influence of different transition measures on the dynamic response index of vehicle-track system, and then reasonable measures for setting the ballasted-ballastless transition sections are proposed.

5.1. Model Establishment and Parameter Value. The vehicle is selected as CRH2, which is regarded as a multi-rigid body system composed of body, frame, and wheelset. The heave and nodding degrees of the car body and the front and rear frame are considered. The wheelset only considers the heave degree of freedom. The wheel-rail normal force is determined by Hertz nonlinear elastic contact theory. Ballasted track is composed of CHN60 rail, elastic strip V fastener, type III concrete sleeper, and ballasted track bed, and the fastener spacing is 0.6 m. The double block ballastless track is composed of CHN60 rail, WJ-8B fastener, track bed plate, and supporting layer and the fastener spacing is 0.65 m. According to the respective structural characteristics of ballasted track and ballastless track, the vehicle-track mechanical model is established, as shown in Figure 5. In the model, the rail and sleeper are simplified as Timoshenko beams, and the fasteners are simplified as vertical springs and dampers. The ballasted track bed is simplified as multi-spring damper and multi-row mass block.

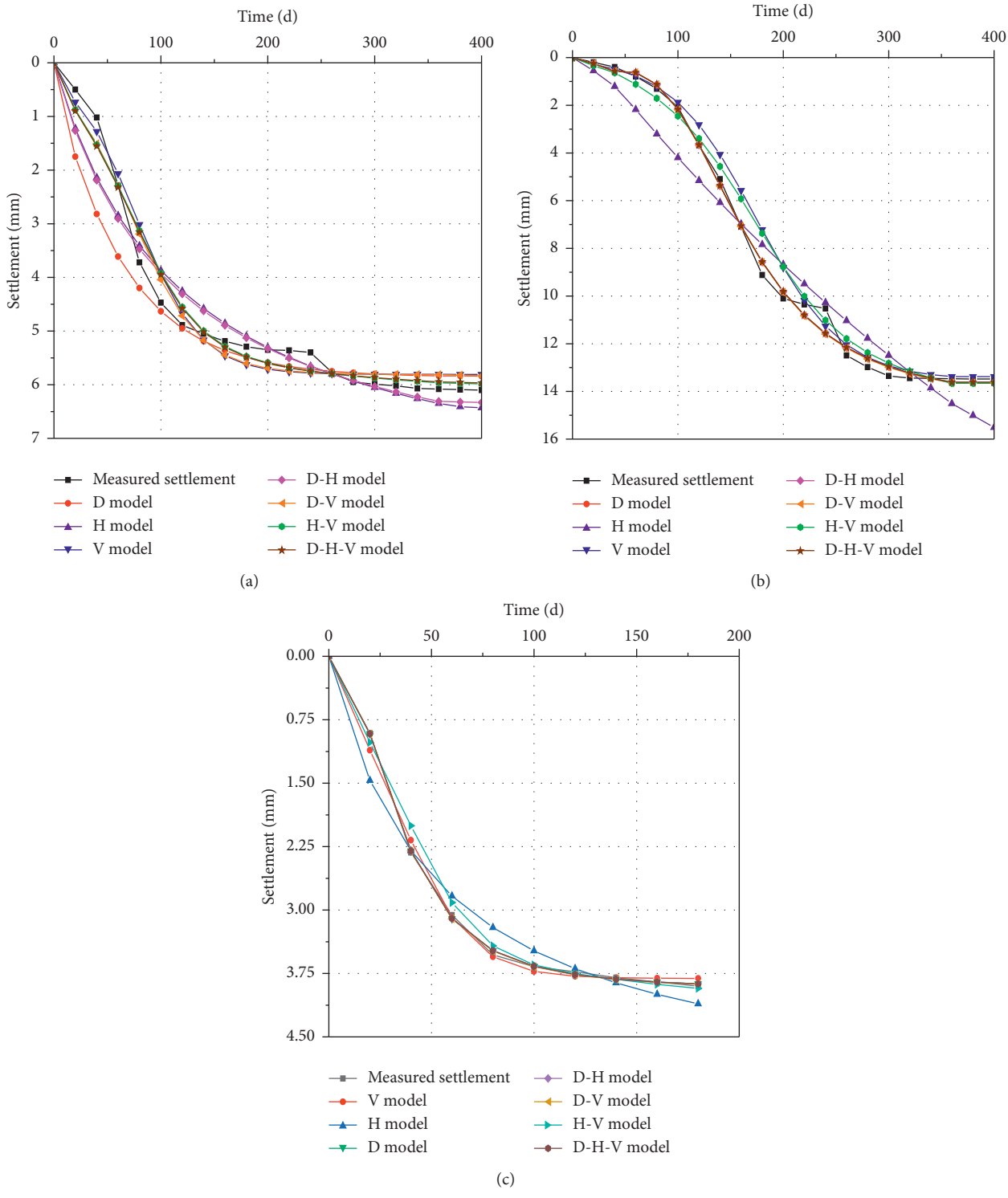

Figure 2: Curves of measured settlement and predicted settlement. (a) DK84 + 771 section. (b) DK84 + 821 section. (c) DK123 + 960 section.

5.2. Setting Scheme of Transition Section

5.2.1. Graded Transition of Fastener Stiffness. In order to ensure the safe and smooth passage of high-speed trains through the transition section and reduce the impact and vibration of wheel and rail, the three-stage fastener stiffness is set within the length of ballasted-ballastless transition section. In this paper, the length of ballasted-ballastless transition section is 30 m, that is, from the beginning of the ballasted track, the fastener stiffness is gradually reduced by three sections, and the length of each section is 10 m.

In order to eliminate the boundary effect, the length of ballasted track section is 90 m and that of the ballastless track section is 130.66 m in the model. The vertical stiffness of

Table 5: Comparison of precision index values of each prediction model.

Model	Beitan station										Pingchuan station				
	DK84 + 771 section					DK84 + 821 section					DK123 + 960 section				
	SSE	SE	SSPE	SPE	MAPE/%	SSE	SE	SSPE	SPE	MAPE/%	SSE	SE	SSPE	SPE	MAPE/%
D型	7.4918	0.5973	9.7202	0.6803	26.35	2.3866	0.3371	0.3611	0.1311	7.34	0.0791	0.0889	0.0535	0.0731	3.63
H型	3.7412	0.4221	3.4330	0.4043	17.30	30.5082	1.2053	13.6796	0.8071	45.99	0.5722	0.2392	0.3980	0.1995	9.55
V型	2.0469	0.3122	0.3780	0.1342	8.58	10.7258	0.7147	0.4410	0.1449	9.73	0.0069	0.0260	0.0006	0.0080	0.64
D-H	3.6075	0.4049	3.7866	0.4246	17.51	2.3639	0.4049	0.3611	0.1311	7.31	0.0068	0.4049	0.0007	0.0081	0.65
D-V	1.8520	0.2970	0.8836	0.2051	10.15	2.3725	0.3361	0.3626	0.1314	7.31	0.0068	0.0261	0.0007	0.0081	0.66
H-V	1.5884	0.2750	0.8734	0.2039	9.40	8.7031	0.6438	1.2390	0.2429	14.95	0.0059	0.0243	0.0006	0.0079	0.65
D-H-V	1.5827	0.2754	0.9438	0.2120	9.73	2.3630	0.3354	0.3601	0.1310	7.31	0.0067	0.0260	0.0007	0.0081	0.65

fasteners in ballasted track segment is 60 kN/mm, and the damping is 75 kN s/m. The vertical stiffness of fasteners in ballastless track segment is 25 kN/mm, and the damping is 75 kN s/m. The vertical stiffness of the fastener in the transition section is divided into three sections. The stiffness of each section is 35 kN/mm, 45 kN/mm, and 55 kN/mm, respectively, and the damping is constant. The vertical stiffness and damping of the ballast track bed are 120 kN/mm and 60 kN s/m, respectively. The surface layer of subgrade bed is graded gravel, and the bottom and below subgrade of subgrade bed are group B fillers. In this paper, the comprehensive stiffness of subgrade is selected as 180 kN/mm.

5.2.2. Ballast Glue Graded Curing Ballast Bed Transition. Ballast glue curing ballast bed technology is a new type of transition section treatment measures to realize ballast particle bonding and improve the overall stiffness of ballast bed by field spraying ballast glue. The binder is a nontoxic and harmless polyurethane material, which is an environmentally friendly binder. During line maintenance and repair, ballast particles can be re-dispersed directly through manual or large machine operation. After the line maintenance is completed, the ballast glue is sprayed again to form a solidified ballast bed.

The ballast glue is used to solidify the ballast bed in sections within the length of the transition section. That is, starting from the ballast track section, the ballast bed is solidified in three stages (local section consolidation, partial section consolidation, and full section consolidation, respectively), and the stiffness of the ballast bed is gradually increased. The length of the solidified ballast bed in each stage is 10 m, and the total length of the transition section is 30 m.

The full section consolidation scheme solidified the track bed under the sleeper, the track bed in the sleeper box, and the track bed in the shoulder ballast part, and the curing thickness under the sleeper was 275 mm. The partial section consolidation scheme mainly solidifies the ballast bed under the sleeper and the ballast bed of the shoulder. The bond thickness under the sleeper is 225 mm, and the bond thickness of the ballast shoulder is 100 mm. The local section consolidation scheme only solidifies the track bed under the sleeper, and the bonding thickness of the sleeper bottom is 225 mm. The error of bond thickness should be controlled at ±25 mm.

The ballast glue curing ballast bed technology can change the mechanical properties of ballast bed, effectively improving the support stiffness of ballast bed, and showing good rebound characteristics. According to the test results of reference [22–25], the vertical stiffness of the local section consolidated ballast bed is 140 kN/mm, the vertical stiffness of the partial section consolidated ballast bed is 200 kN/mm, and the vertical stiffness of the full section consolidated ballast bed is 290 kN/mm.

5.3. Track Irregularity. The actual track irregularity is affected by many factors, including the initial bending of the rail, rail wear, damage, uneven quality, uneven track bed gradation and strength, looseness, dirt, slab, uneven subgrade subsidence, and stiffness change. The combined action of the above factors constitutes the track's irregularity characteristics [26–29]. The vehicle and track structure will vibrate under the excitation of the track's irregularity. On the one hand, it will affect the comfort of passengers. On the other hand, it will affect the fatigue damage and operation reliability of vehicle and track structure components. Combined with the engineering practice, this paper selects the measured vertical track irregularity of a section in Yinchuan-Zhongwei high-speed railway as the model input to carry out the vehicle-track coupling dynamic analysis, as shown in Figure 6.

5.4. Analysis of Calculation Results. The dynamic response analysis of two transition measures is carried out by vehicle-track coupling analysis program. The response indexes of vehicle body acceleration, wheel load reduction rate, wheel-rail force, wheel acceleration, rail acceleration, and rail vertical displacement are calculated, respectively, and the variation law of each index is analyzed. Due to space limitations, except the car body acceleration, this paper only lists the dynamic response results under the first wheelset, as shown in Figures 7 and 8. The maximum dynamic response of the vehicle-rail system is shown in Table 7.

Figures 7 and 8 are the dynamic response curves of the vehicle-rail system under the conditions of fastener stiffness

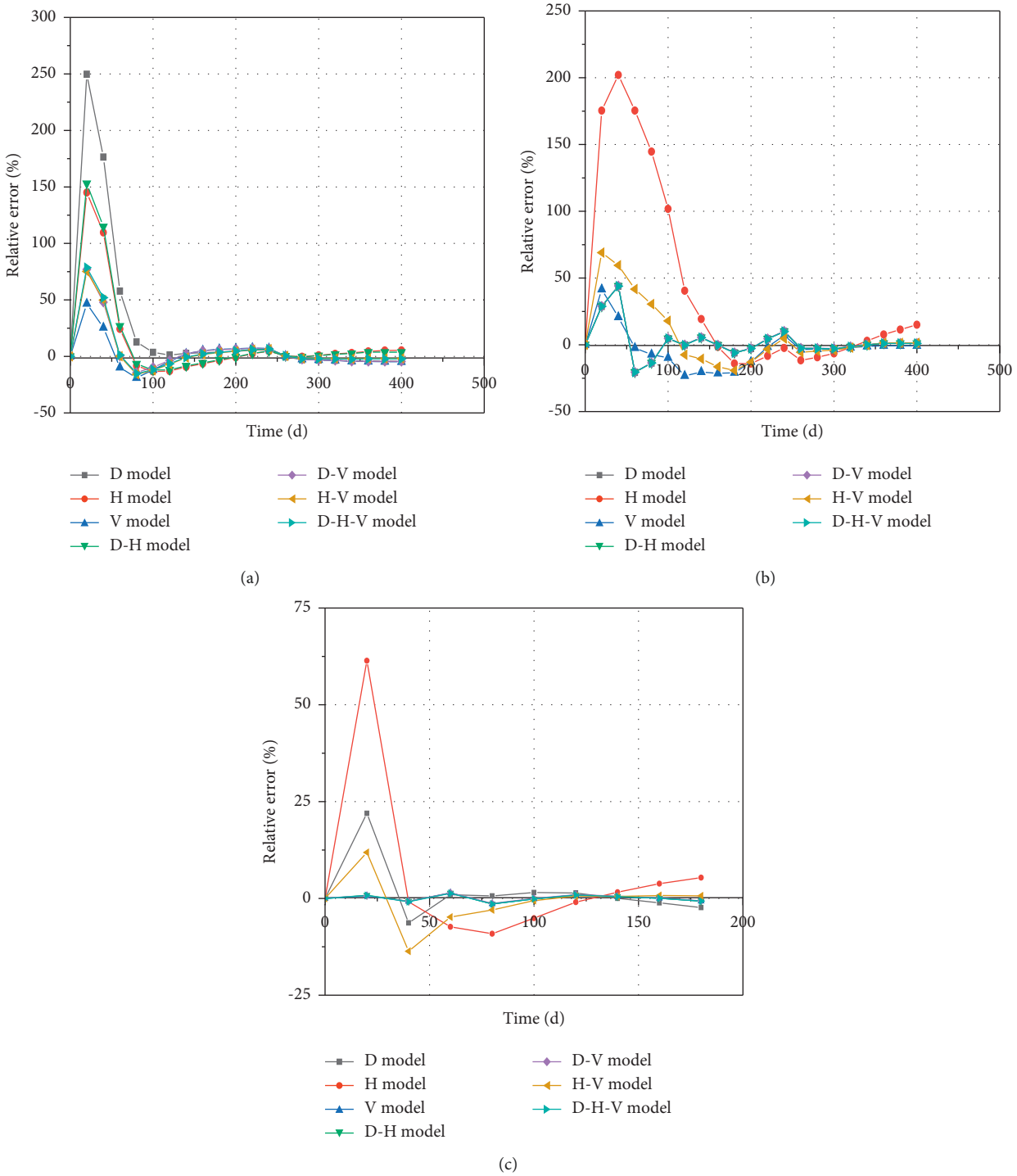

Figure 3: Observation time and relative error curves. (a) DK84 + 771 section. (b) DK84 + 821 section. (c) DK123 + 960 section.

transition and ballast glue curing track bed transition. It can be seen that under the measured irregularity conditions, the vertical vibration accelerations of the two transition modes are basically the same, and the maximum values are close, both less than 0.3 m/s^2, indicating that the two transition modes have little influence on the vertical acceleration of the car body. When the fastener stiffness transition is adopted, the comprehensive stiffness of the track is greater than that of the ballast glue transition mode, resulting in a large wheel-rail force in the transition section. When the ballast glue transition is adopted, the maximum wheel-rail force occurs outside the transition section and just enters the ballastless track section. The two transition modes have little influence on wheelset acceleration and rail vibration acceleration, but have great influence on rail dynamic displacement. When the fastener stiffness transition is adopted, the rail dynamic

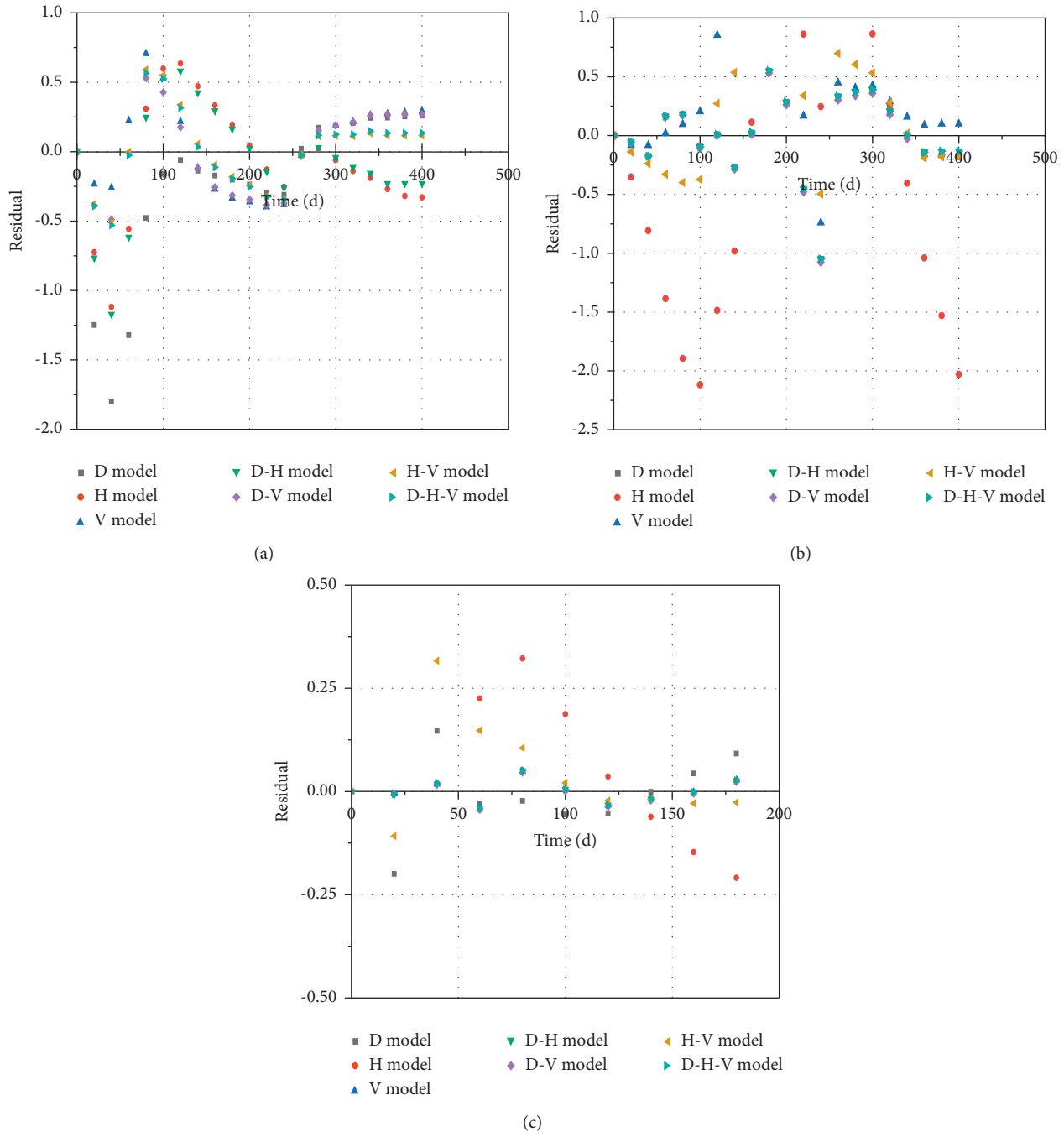

Figure 4: Observation time and residual scatter plots. (a) DK84 + 771 section. (b) DK84 + 821 section. (c) DK123 + 960 section.

Table 6: Post-construction settlements (mm).

Mileage	Prediction model	Current settlement	Final settlement	Post-construction settlement
DK84 + 771	D-H-V	6.1	6.44	0.34
DK84 + 821	D-H-V	13.48	14.44	0.96
DK123 + 960	D-H-V	3.90	3.93	0.03

displacement increases gradually in the ballast track section and it reaches a large value after entering the transition section and then remains basically unchanged. When the ballast glue is used to solidify the ballast bed transition, it is just the opposite to the stiffness transition of the fasteners. It gradually decreases from the ballast section to a certain

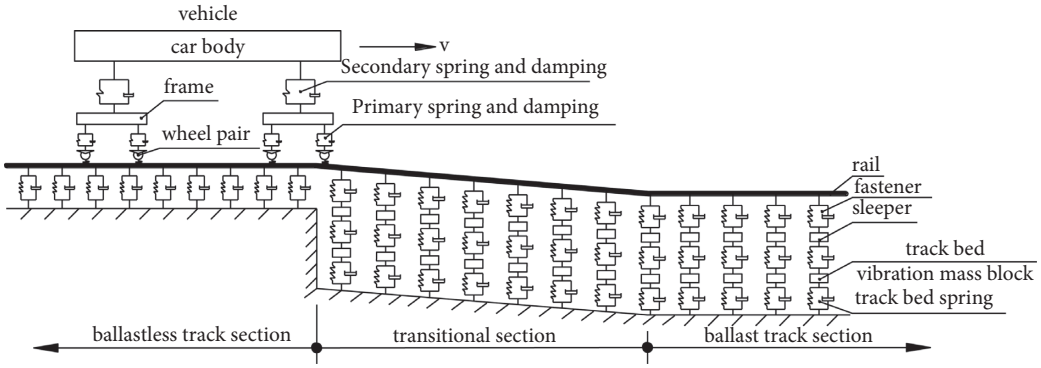

Figure 5: Vehicle-track dynamics model.

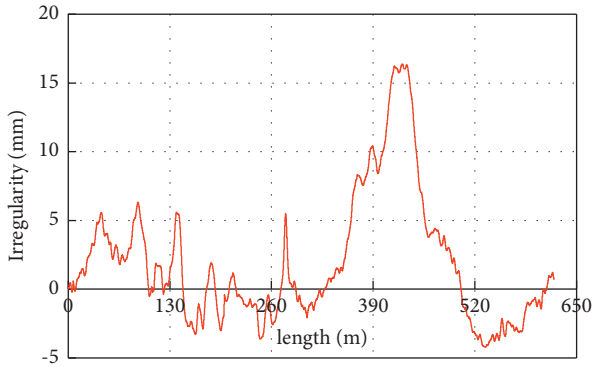

Figure 6: Vertical irregularity of track.

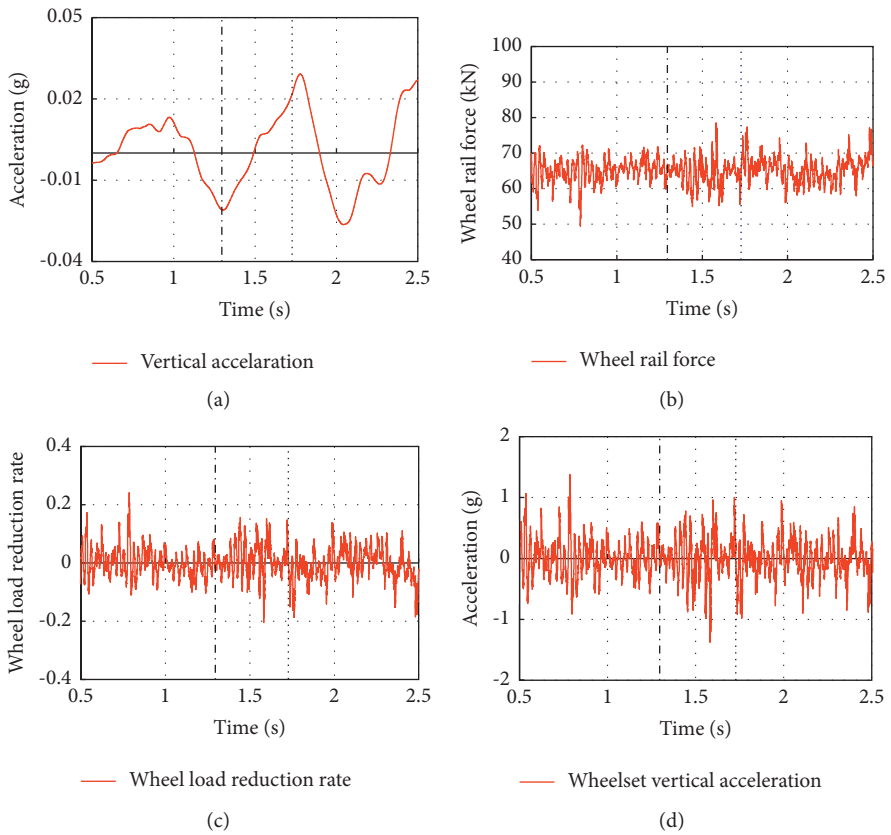

Figure 7: Continued.

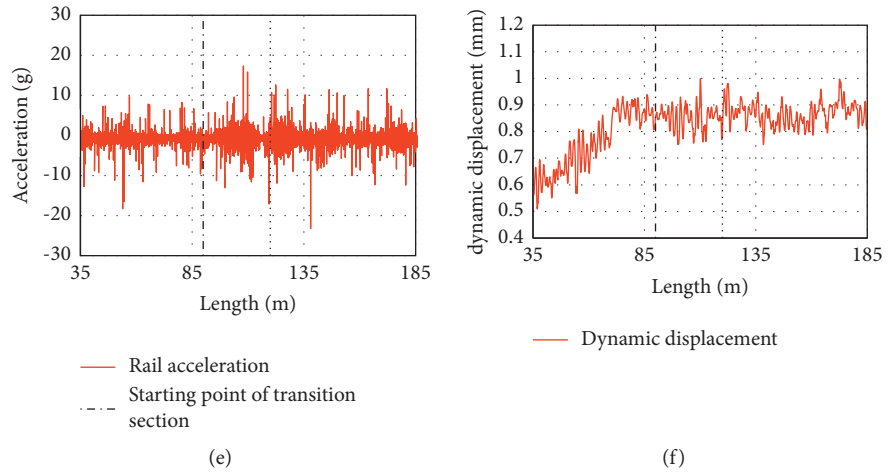

Figure 7: Dynamic response curve of vehicle-rail system under fastener stiffness transition. (a) Vertical acceleration of vehicle body. (b) Wheel-rail force. (c) Wheel load reduction rate. (d) Wheelset vertical acceleration. (e) Rail vertical acceleration. (f) Rail dynamic displacement.

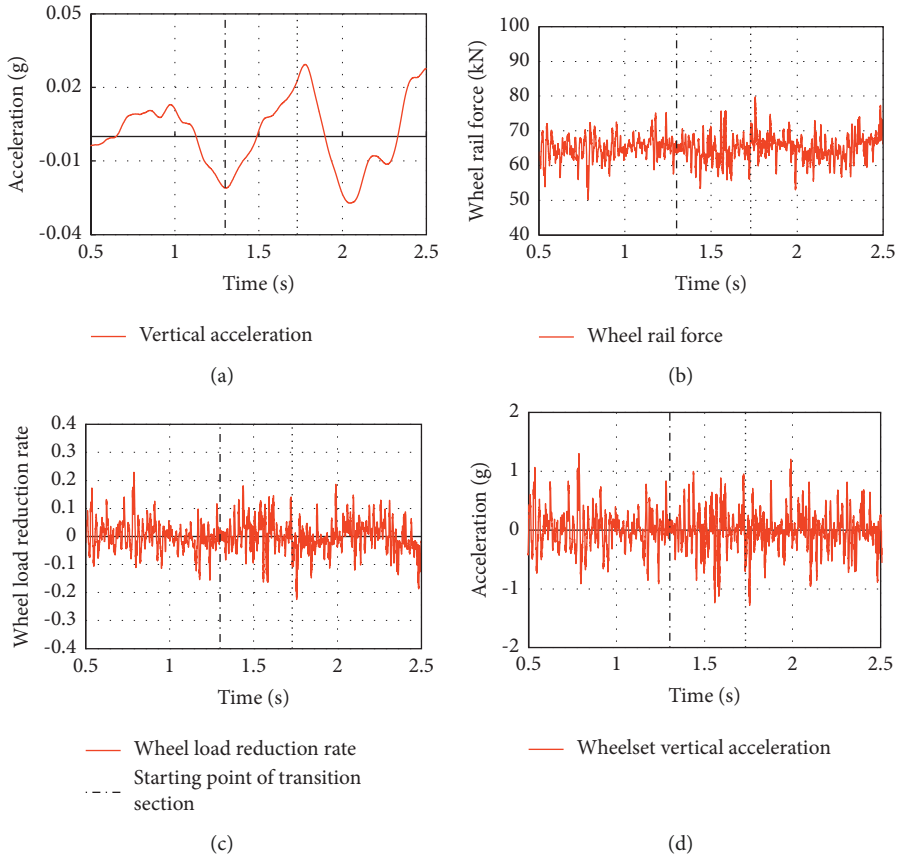

Figure 8: Continued.

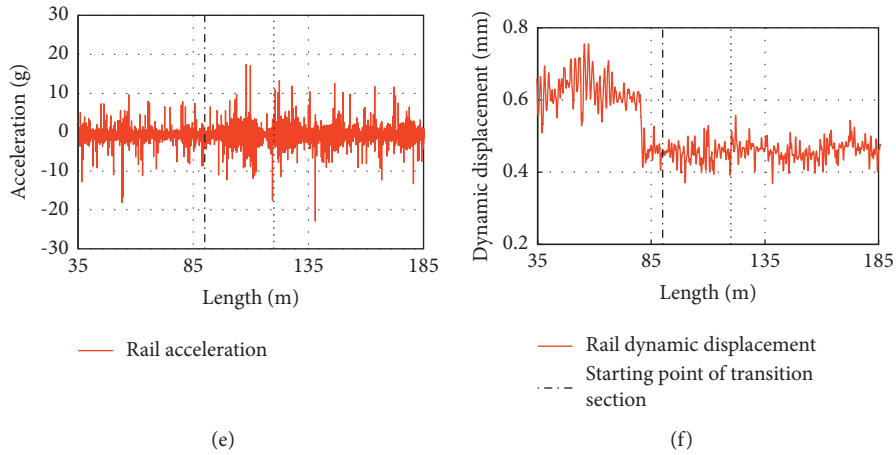

Figure 8: Dynamic response curve of vehicle-rail system under ballast glue cured track bed. (a) Vertical acceleration of vehicle body. (b) Wheel-rail force. (c) Wheel load reduction rate. (d) Wheelset vertical acceleration. (e) Rail vertical acceleration. (f) Rail dynamic displacement.

Table 7: Summary of the maximum dynamic response of vehicle-rail system.

Transitional measures	Vehicle acceleration/m s^{-2}	Wheel-rail force/kN	Wheel unloading rate	Wheelset acceleration/m s^{-2}	Rail acceleration/ m s^{-2}	Rail dynamic displacement/mm
Fastener stiffness transition	0.292	78.4	0.241	13.8	232.5	0.998
Ballast glue curing track bed transition	0.294	79.8	0.229	13.0	228.8	0.756
Evaluation criteria	≤1.30	≤170	≤0.60	—	≤5000	≤2.0

stable value before entering the transition section, and the subsequent change is small. It can be seen from Table 5 that the dynamic response index values of vehicles and track structures under the two transitional measure modes are not so different, and both are less than the evaluation criteria of "the Technical Specifications for Dynamic Acceptance of High-speed Railway Engineering" [30], and it can be guaranteed that the value does not exceed the limit value, which can ensure the high-speed, safe, and smooth passage of the train. However, the fastener stiffness transition measures are simple, convenient, and easy to replace. Therefore, it is recommended to adopt the fastener stiffness transition measures in the ballasted-ballastless transition section.

6. Conclusions

Based on the engineering background of laying ballastless track in the high embankment turnout areas of the Beitan Station and the Pingchuan Station of the Zhonglan high-speed railway, this paper studies the relevant technical problems and draws the following conclusions:

(1) Based on the design standards of the ballast track subgrade, combined with the site subgrade filling progress, in order to reduce the post-construction settlement of station turnout subgrade and meet the conditions of laying ballastless track, a detailed subgrade reinforcement scheme is proposed.

(2) In order to make up for the deficiency of the single settlement prediction model in the settlement prediction of high-fill subgrade, this paper conducts the optimal combination based on the grey Verhulst, hyperbola, and Deng Yinger prediction model and deduces the combined prediction model.

(3) The combination models of two-models and three-models are constructed. Combined with the settlement monitoring data, the subgrade settlement is predicted. The comparative analysis of five accuracy evaluation parameters shows that the accuracy of the three-model combination prediction model is better than that of any single-model and two-model combination model, and their reliability and adaptability are stronger. Especially, when the monitoring time exceeds the inflection point of the curve, it is almost close to the measured value. Therefore, the optimal combination prediction model has a certain reference value in settlement prediction.

(4) The combined prediction model proposed in this paper can be applied to the optimal combination of multiple models, which can cover the advantages and disadvantages of each single model and greatly improve the accuracy of settlement prediction.

(5) Based on the optimal settlement prediction model, the settlement of high-fill subgrade in the turnout areas of the stations is predicted. The calculation

results show that the post-construction settlement of the three sections is less than 15 mm, which meets the requirements of laying ballastless track.

(6) The dynamic analysis model of the vehicle and ballasted-ballastless track transition section is established. According to the two measures of fastener stiffness grading transition and ballast glue curing ballast bed grading transition, the vehicle-track dynamic response analysis shows that the dynamic response indexes of vehicle-track system under the two transition modes are not exceeded, which meets the requirements for the smooth passing of high-speed trains. Taking into account that the fastener stiffness transition measures are simple, construction is convenient, and replacement is easy, therefore the fastener stiffness transition measures is recommended.

Data Availability

The data used to support the findings of this study are included within the article.

Conflicts of Interest

The authors declare that they have no conflicts of interest.

Authors' Contributions

Xue Ning Ma performed the technological development. Zi Xiang Hao and Chang Liu edited the manuscript and did data processing. Zi-Xiang Hao and Chang Liu contributed equally to this work and should be considered co-first authors.

Acknowledgments

This work was financially supported by the National Natural Science Foundation of China (Grant no. 41562014) and the Project of Science and Technology Research and Development Plan of China Railway Lanzhou Bureau Group Co., Ltd. (lj20210922-3397).

References

[1] R. J. Li, Z. P. Han, C. X. Wei, H. Xiao, and P. Wang, "Analysis and treatment of turnout defects on shen-shuo heavy haul railway," *Railway Standard Design*, vol. 58, no. 9, pp. 28–32, 2014.

[2] G. C. Zou, "Seamless transformation of turnout area of speed increasing line," *Railway Engineering*, vol. 45, no. 5, pp. 83-84, 2005.

[3] K. Ren, *Research on Rail Grinding Technology in Turnout Area of normal Speed Railway*, China Academy of Railway Sciences, 2020.

[4] *TB10621-2014*, Code for Design of High Speed Railway, 2014.

[5] Z. J. Feng and W. H. Cao, "Observation and numerical analysis of settlement of high fill embankment on soft foundation," *Journal of Lanzhou University of Technology*, vol. 39, no. 2, pp. 126–129, 2013.

[6] Z. W. Liu, X. Han, C. Y. Chen, and J. Jia, "Semi-numerical and semi-analytical method for predicting settlement of high embankment," *Journal of Underground Space and Engineering*, vol. 7, no. 3, pp. 491–496, 2011.

[7] H. P. Feng, H. L. Geng, B. W. Han, W. D. Shang, and J. M. Chang, "Prediction model for subgrade settlement of high speed railway in unsaturated soil region," *Journal of Geotechnical Engineering*, vol. 39, no. 6, pp. 1089–1095, 2017.

[8] A. Siew, "Hyperbolic method for settlement in clays with verticaldrains," *Canadian Geotechnical Journal*, vol. 31, no. 1, pp. 125–131, 1994.

[9] A. Akira, "Observational procedure of settlement predictions," *Soils and Foundations*, vol. 18, no. 4, pp. 87–101, 1978.

[10] S. A. Tan and S. H. Chew, "Comparison of the hyperbolic and Asaoka observational method of monitoring consolidation with vertical drains," *Soils and Foundations*, vol. 36, no. 3, pp. 31–42, 1996.

[11] C. H. Zhu, N. Li, M. Z. Liu, and W. E. I. Yi-feng, "Temporal and spatial analysis of post-construction settlement of loess high fill foundation at Lv-Liang airport," *Journal of Geotechnical Engineering*, vol. 35, no. 2, pp. 293–301, 2013.

[12] X. W. Lei, S. W. Bai, and Q. S. Meng, "Application of grey prediction in settlement analysis of soft soil foundation," *Rock and Soil Mechanics*, vol. 21, no. 2, pp. 145–147, 2000.

[13] Y. H. Song and D. X. Nie, "Verhuslst model for prediction of foundation settlement," *Rock and Soil Mechanics*, vol. 24, no. 1, pp. 123–126, 2003.

[14] H. B. Liu, Y. M. Xiang, and Y. X. Ruan, "Application of multivariable grey model with optimized background value in subgrade settlement prediction," *Rock and Soil Mechanics*, vol. 34, no. 1, pp. 173–181, 2013.

[15] Q. Wang, H. Yan, X. Q. Yuan, N. Cen, and Z. Xudong, "Settlement prediction of dredger fill with the optimal combination model," *Journal of Donghua University*, vol. 31, no. 6, pp. 812–816, 2014.

[16] T. Niu, L. Zhang, S. Wei, B. Zhang, and B. Zhang, "Study on a combined prediction method based on BP neural network and improved verhulst model," *Systems Science & Control Engineering*, vol. 7, no. 3, pp. 36–42, 2019.

[17] B. Wang, X. Wang, and X. Ma, "Study on optimal combination settlement prediction model based on logistic curve and Gompertz curve," *Stavební obzor - Civil Engineering Journal*, vol. 29, no. 03, pp. 347–357, 2020.

[18] P. Wang and Y. W. Ju, "Study on logistic hyperbolic combination model for prediction of settlement of high loess filling embankment," *Highways*, vol. 63, no. 4, pp. 12–17, 2018.

[19] C. Lin, G. Feng, and W. Zishuo, "An optimal combination prediction method of turnover spare parts consumption based on certain weight," *Journal of Physics: Conference Series*, vol. 1955, no. 1, Article ID 12122, 7 pages, 2021.

[20] T. H. Rhee and K. H. Ryu, "Crowd sourcing of economic forecast: combination of combinations of individual forecasts using bayesian model averaging," *Seoul Journal of Economics*, vol. 34, no. 1, pp. 1–15, 2021.

[21] W. Qi, "Application of ballast glue curing track bed technology in transition section of ballastled- ballastless track," *China Railway*, vol. 12, pp. 47–51, 2016.

[22] Y. Deng and H. P. Xie, "New model and method of forecasting settlement during complete process of construction and operation," *Rock and Soil Mechanics*, vol. 1, pp. 1–4, 2005.

[23] X. W. Tang, "Optimal combination prediction method and its application," *Mathematical Statistics and Management*, vol. 1, pp. 31–35, 1992.

[24] S. S. Zhai and J. Duan, "Simulation comparison analysis of combination weight determination method," *Statistics & Decisions*, vol. 24, pp. 83–85, 2015.
[25] Y. J. Zhu, "The key control technology of ballast rubber applied in the transition section of ballasted-ballastless track," *Railway Engineering*, vol. 56, no. 8, pp. 133–136, 2016.
[26] Y. J. Zhu, W. Qi, and P. Chen, "Research on the influenced of ballast glue in transitions on parameters of ballast bed," *Journal of Railway Science and Engineering*, vol. 13, no. 1, pp. 34–39, 2016.
[27] W. Qi, Y. T. Liu, and C. H. Li, "Dynamic testing and analysis of ballasted track of different stiffness sections using polyurethane ballast reinforcement technique," *Journal of Central South University*, vol. 49, no. 3, pp. 764–770, 2018.
[28] B. Wang and J. R. Bao, "Study on the influence of ballast glue on track bed parameters," *Railway Standard Design*, vol. 11, pp. 14–16, 2010.
[29] X. Ling and H. Xiao, "Experimental study and discrete element analysis on mechanical properties of glued ballast with different glue consumption," *Journal of the China Railway Society*, vol. 41, no. 10, pp. 107–114, 2019.
[30] *TB10761-2013, Technical Regulations for Dynamic Acceptance for High-Speed Railways Construction*, 2013.